Quantum instability in a dc SQUID with strongly asymmetric dynamical parameters

A. U. Thomann,[1] V. B. Geshkenbein,[1,2] and G. Blatter[1]
[1]*Institute for Theoretical Physics, ETH Zurich, 8093 Zurich, Switzerland*
[2]*L. D. Landau Institute for Theoretical Physics, 117940 Moscow, Russia*
(Received 22 December 2008; revised manuscript received 19 March 2009; published 15 May 2009)

A classical system cannot escape out of a metastable state at zero temperature. However, a composite system made from both classical and quantum degrees of freedom may drag itself out of the metastable state by a sequential process. The sequence starts with the tunneling of the quantum component which then triggers a distortion of the trapping potential holding the classical part. Provided this distortion is large enough to turn the metastable state into an unstable one, the classical component can escape. We show that such a composite system can be conveniently studied and implemented in a dc superconducting quantum interference device (SQUID) featuring asymmetric dynamical parameters. We determine the dynamical phase diagram of this system for various choices of junction parameters and system preparations.

DOI: 10.1103/PhysRevB.79.184515 PACS number(s): 85.25.Dq, 74.50.+r

I. INTRODUCTION

Consider a classical object (a heavy degree of freedom) trapped in a metastable potential minimum; no decay out of this metastable state is possible at low temperatures, where thermal activation over the barrier is exponentially suppressed. However, if the classical object is a composite one, with a quantum object (a light degree of freedom) coupled to the classical one, then the quantum object may tunnel out of the metastable minimum and exert a pulling force on the classical one. Once this force is large enough to completely suppress the trapping barrier, the classical object is able to leave the potential well—hence a classical object may escape from a metastable state even at zero temperature if helped by a coupled quantum degree of freedom. This process reminds of the famous Baron Münchhausen who told the story of rescuing himself from sinking in a swamp by pulling himself up by his own hair—we thus term this decay the "Münchhausen effect."

The above situation can be realized in a dc superconducting quantum interference device (SQUID) featuring asymmetric dynamical parameters, i.e., with two Josephson junctions of equal critical currents J_c but strongly different (shunt) capacitances C and (shunt) resistances R (see Fig. 1). Choosing large and small parameters C and $1/R$ for the two junctions allows to place one of the junctions in the "classical" and the other into the quantum domain. The tunneling of the quantum degree of freedom entails a distortion of the trapping potential of the classical junction, which might be sufficiently large to transform the metastable state of the classical junction into an unstable one. The appearance of this complex decay channel depends critically on the applied bias current J and the SQUID's loop inductance L coupling the two junctions.

The gauge-invariant phase differences φ_i, $i=1,2$, across the two Josephson junctions[1] define our dynamical degrees of freedom: assuming equal critical currents J_c, the junctions' potential energies $\mathcal{V}_i=E_J[1-\cos\varphi_i]$, $i=1,2$, involve the Josephson energy $E_J=\Phi_0 J_c/2\pi c$ (with $\Phi_0=hc/2e$ the flux unit, e and c denote the unit charge and light velocity).[2] Their kinetic energies $\mathcal{T}_i=(\hbar/2e)^2 C_i\dot{\varphi}_i^2/2$ are determined by the junction capacitances C_i playing the role of effective masses (the relevant energy scale is given by the charging energy $E_{c,i}=e^2/2C_i$)—a dynamically asymmetric SQUID with one large and one small junction capacitance then provides us with the desired classical and quantum degrees of freedom (we choose $C_1 \gg C_2$; additional normal resistances R_i introduce a dissipative dynamical component, see below). The coupling of the two junctions via the loop inductance L produces the interaction energy $\mathcal{V}_{\rm int}=[(\Phi_0/2\pi)^2/2L](\varphi_2-\varphi_1)^2$ involving the relative coordinate $(\varphi_2-\varphi_1)$, whereas the external driving current J couples to the absolute coordinate, $\mathcal{V}_{\rm drive}=E_J(J/2J_c)(\varphi_1+\varphi_2)$. While large-capacitance (classical) junctions are easily fabricated, small (quantum) junctions are more difficult to realize. Nevertheless, experimental techniques to fabricate small junctions are available today and their quantum behavior in the form of quantum tunneling,[3–6] quantized energy levels,[7,8] and even quantum coherence[9–15] has been demonstrated.

The quantum decay of the biased, dynamically symmetric dc SQUID has been discussed before both experimentally[16,17] and theoretically,[18] also in the context of instanton splitting.[19,20] In the SQUID discussed here,[21] the large asymmetry of the dynamical parameters blocks the tunneling of the φ_1 degree of freedom since the tunneling rate is

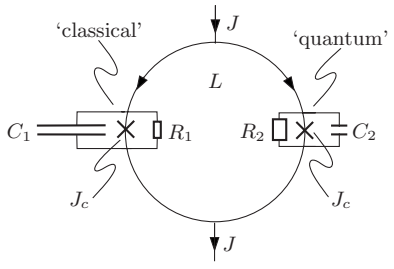

FIG. 1. Schematics of the dynamically asymmetric dc SQUID. Two Josephson junctions are integrated in a current (J) biased superconducting loop with inductance L. The two junctions feature equal critical currents J_c but strongly asymmetric (shunt) capacitances C_i and (shunt) resistances R_i. We assume that C_i and R_i are chosen such that quantum effects are present for junction 2 but are strongly suppressed for junction 1, hence $C_1 \gg C_2$ and/or $R_1 \ll R_2$.

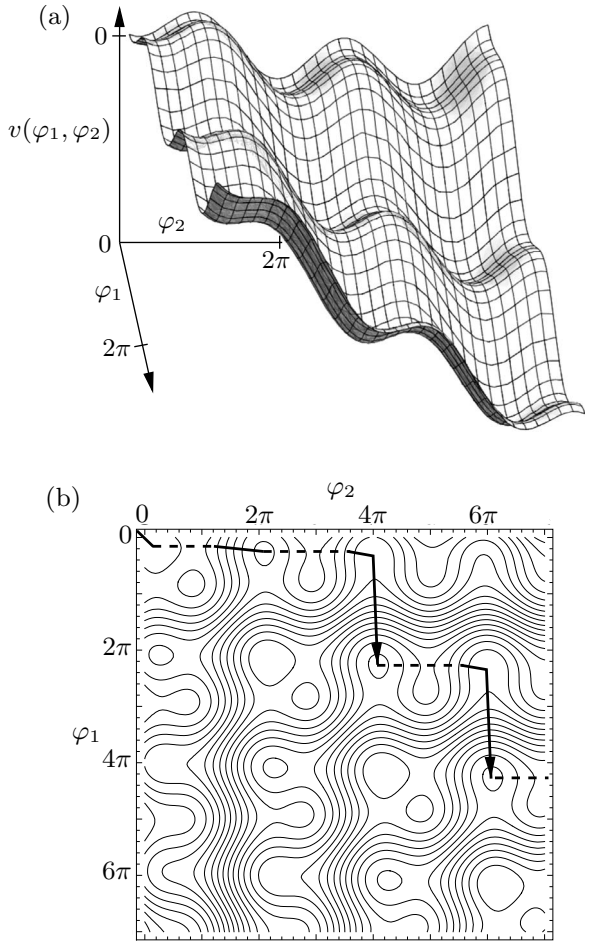

FIG. 2. (a) Surface and (b) contour plot of the SQUID potential, Eq. (2), at bias current $j=0.5$ and coupling $k=0.04$. For an undercritical current $j<1$, the symmetric minima ($\varphi_1=\varphi_2$) are all metastable. The stability of the side minima ($\varphi_1\neq\varphi_2$) depends crucially on the parameters j and k. The line in (b) shows the decay path in an overdamped setup: the system starts out in a relaxed local ground state near the initial minimum at $\varphi_1=\varphi_2=\arcsin j$. The light degree of freedom φ_2 then tunnels (dotted line) and the system relaxes to the bottom of the next minimum near $\varphi_2\approx 2\pi$, with a classically stable but quantum mechanically metastable ground state. Through an additional quantum phase slip, the light phase reaches the minimum near $\varphi_2\approx 4\pi$, which is *not* classically stable and henceforth the system can decay along a classically allowed path to $\varphi_1\approx 2\pi$. The system then has turned unstable and enters a resistive state through iteration of the last two steps.

exponentially suppressed with an exponent $\propto(E_J/E_c)^{1/2}$. The "heavy" junction then remains frozen during the quantum decay of the "light" degree of freedom φ_2. A trajectory of this kind describes the entry of flux into the SQUID loop which rearranges the current flow in the two arms in a way as to redirect more current through the heavy junction. This increase in current produces an enhanced tilt $-J_{\rm eff}\varphi_1$ in the potential of the heavy junction, which then may decay through a classical trajectory (see Fig. 2). We call this nontrivial decay sequence the "Münchhausen decay." It is the aim of this work to determine the effective critical current $J_c(L^{-1})$ for which the Münchhausen decay becomes possible (see Figs. 5 and 9–12).

In the following, we define our system in full detail, including a dissipative component in the junction dynamics (Sec. II). Sections III and IV are devoted to the derivation of the effective critical currents for the various cases with junctions governed by massive or dissipative dynamics. In Sec. V we add remarks concerning the experimental realization of the system described here. Finally, we draw conclusions in Sec. VI.

II. SETUP AND MODEL

Within the resistively and capacitively shunted junction (RCSJ) model (at $T=0$), the classical dynamics of the two phase differences φ_1 and φ_2 is governed by the equations of motion

$$\omega_{0,i}^{-2}\ddot{\varphi}_i+\eta_i\dot{\varphi}_i=-\partial_{\varphi_i}v(\varphi_1,\varphi_2), \tag{1}$$

with the plasma frequency $\hbar^2\omega_{0,i}^2=8E_JE_{c,i}$ of an unbiased single junction and the damping coefficients $\eta_i=\Phi_0/2\pi cJ_cR_i$ (R_i denote the normal Ohmic junction resistances). The potential (see Fig. 2) is given by

$$v(\varphi_1,\varphi_2)=1-\cos\varphi_1+1-\cos\varphi_2-j(\varphi_1+\varphi_2)+\frac{k}{2}(\varphi_1-\varphi_2)^2, \tag{2}$$

with the dimensionless current $j=J/2J_c$ and the coupling constant $k=\Phi_0c/2\pi J_cL=1/\beta_L$ (β_L denotes the usual screening parameter of the SQUID). Equations (1) and (2) describe a dc SQUID with symmetric inductance L in a vanishing external magnetic field and driven by a bias current J or, equivalently, the massive (mass $\propto\omega_{0,i}^{-2}$) and/or dissipative (η_i) dynamics of two harmonically (k) coupled particles in a tilted (j) and corrugated ($\cos\varphi_i$) potential. Quantum effects of the light junction 2 are accounted for via the relevant tunneling and decay processes (see below).

For large $k\gg 1$, the potential $v(\varphi_1,\varphi_2)$ strongly couples the two degrees of freedom and their relative motion is inhibited. The effects we are interested in here emerge in the regime $k<1$, where φ_1 and φ_2 can separate. Then, the potential (2) gives rise to two types of relevant frequencies. One is the plasma frequency $\omega_{p,i}$, the small-amplitude frequency in the direction of φ_i around a local minimum of the potential $v(\varphi_1,\varphi_2)$. With the effective potential

$$v_{\rm eff}[\varphi_l](\varphi_i)=v(\varphi_l=\text{const},\varphi_i),\quad i\neq l, \tag{3}$$

(cf. Fig. 3) $\omega_{p,i}^2=\omega_{0,i}^2\partial_{\varphi_i}^2v_{\rm eff}(\varphi_i)$, evaluated at a local minimum $\varphi_i^{\rm min}$, and depends on the parameters j and k as well as on $\varphi_i^{\rm min}$. For the heavy junction (junction 1), $\omega_{p,1}$ can become arbitrarily small upon approaching criticality, while for the quantum junction (junction 2) $\omega_{p,2}$ becomes small only for $j\to 1$ and $k\to 0$. The other frequency is given by the LC constant of the "superwell" in $v_{\rm eff}(\varphi_2)$ (cf. Fig. 3) and is relevant only in the regime $k\ll 1$ and for the quantum junction (junction 2), $\omega_{LC,2}^2=\omega_{0,2}^2k=c^2/LC_2$.

Using these characteristic frequencies we can delineate the regimes, where the two junctions behave classically and quantum mechanically, respectively. For the heavy junction,

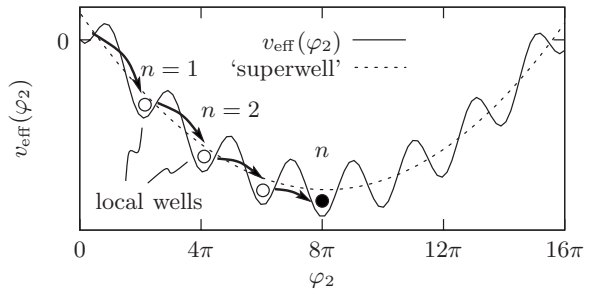

FIG. 3. Effective potential $v_{\rm eff}(\varphi_2)=v(\varphi_1=\text{const},\varphi_2)$ (solid line) and the parabola remaining after dropping $\cos\varphi_2$ (dashed line) for $j=0.5$, $k=0.02$, and $\varphi_1=\arcsin j$. Bullets and arrows illustrate the sequential decay of the quantum phase φ_2 to the ground state for the case of strong damping.

we have to guarantee that the only important quantum effect, tunneling, can be ignored, i.e., that the tunneling rate is sufficiently small. This requires the number $E_b/\hbar\omega_{p,1}\sim(E_J/E_{c,1})^{1/2}(1-|J_1|/J_c)^{5/4}$ of states in the local well to be large, as the tunneling rate for an undamped system (within a cubic approximation of the potential) is $\propto\exp(-36E_b/5\hbar\omega_{p,1})$.[5,22] Here, J_1 is the current through the junction 1. If $|J_1|\to J_c$, the tunneling exponent becomes small, resulting in an observable tunneling rate. However, choosing a large ratio $E_J/E_{c,1}\gg 1$, we can ensure that tunneling effects manifest themselves only close to criticality, where a classical instability is imminent. In this case quantum corrections are small and we can ignore them in our discussion below, i.e., we can treat φ_1 as a classical variable.

For the quantum junction we require $E_J/\hbar\omega_{0,2}$ to be of order unity. Then, the quasiclassical description applies and local wells in $v_{\rm eff}(\varphi_2)$ contain a few quasiclassical states each. Furthermore, tunneling and coherence effects manifest themselves on reasonably short (measurable) time scales.

The strength of dissipation can be quantified by the dimensionless damping parameters

$$\alpha_{p,i}=(2R_iC_i\omega_{p,i})^{-1}, \tag{4}$$

$$\alpha_{LC,2}=(2R_2C_2\omega_{LC,2})^{-1}. \tag{5}$$

Below, we are interested in the two limiting cases of strong and weak damping. For a strongly damped quantum junction with $\alpha_{p,2}>1$, the quantum decay of φ_2 out of a metastable well of $v_{\rm eff}(\varphi_2)$ is incoherent[5,10] and its subsequent relaxation is fast (as compared to the dynamics of φ_1). For weak damping, $\alpha_{LC,2}\ll 1$, $\alpha_{p,i}\ll 1$, the kinetic energy stored in the motion of the heavy junction has to be accounted for; in addition, the finite lifetime of the quantum states of the light junction due to the residual dissipation has to be considered (see the discussion in Sec. IV).

III. STRONG DAMPING

We start our discussion with the simplest case (at least from a theoretical point of view) and analyze the situation for strong damping,[23] $\alpha_{p,2}>1$ and $\alpha_{p,1}\gg 1$ (the normal resistance of good quality junctions vanishes at low temperatures, requiring external shunts to generate damping). We bear in mind an experiment with a dc SQUID characterized by a fixed inductance $L\propto k^{-1}$ and biased with a current $j<1$. The task is to determine whether the Münchhausen decay can take place. In the experiment, the latter manifests itself through the transition to a finite-voltage state. In the strong damping case, no kinetic energy is stored in the system. Furthermore, the evolution is not sensitive to the way the current is ramped. After current ramping, the system starts out in a relaxed state, where the phases φ_i are localized in the diagonal metastable minimum at $\varphi_1=\varphi_2=\arcsin j$ (up to an arbitrary multiple of 2π).

For sufficiently large j, the quantum degree of freedom φ_2 undergoes tunneling to a new local minimum nearby $2\pi n$, while the classical degree of freedom $\varphi_1=\arcsin j$ remains localized, thus allowing a flux $\simeq n\Phi_0$, $n\in\mathbb{N}$, to enter the SQUID loop (cf. Fig. 3). If the resulting force on the classical phase φ_1 is sufficiently large, the Münchhausen decay is enabled with a classical decay of φ_1 and successive iteration of quantum decay (directed along φ_2, flux entry) and classical relaxation (directed mainly along φ_1, flux exit) (cf. Fig. 2).

The strong coupling at large k keeps the local minimum at $\varphi_2=\arcsin j$ lower in energy than the adjacent local well at $\varphi_2\approx 2\pi$ for all bias currents j, hence tunneling is inhibited and no Münchhausen decay takes place. At lower k, a bias current $j<1$ can sufficiently lower the adjacent well such as to bring both minima to equal height. This condition is reached once the minimum of the parabola in $v_{\rm eff}(\varphi_2)$ (at $\varphi_2=\arcsin j+j/k$) is aligned with the midpoint between the two corresponding minima of $-\cos\varphi_2$ (at $\varphi_2=\pi$), i.e., if $\arcsin j+j/k=\pi$. Thus, for $k<k_{c,1}^{+}(j)$, with[24]

$$k_{c,1}^{+}(j)=\frac{j}{\pi-\arcsin j}, \tag{6}$$

the minimum at $\varphi_2\approx 2\pi$ is lower and a quantum decay is enabled [cf. Fig. 4(b), point C in the diagram]. The jump of φ_2 by roughly 2π then pulls the heavy junction out of its minimum and the Münchhausen decay is initiated [cf. Figs. 4(a) and 4(b) associated with the sequence of points A, B, and C in Fig. 4(c)]. The smaller k becomes, i.e., the weaker φ_2 is bound to φ_1, the less current is needed to lower the adjacent minimum such as to allow for a decay of φ_2, hence the positive slope of $k_{c,1}^{+}(j)$.

Decreasing k too far, however, the pulling force exerted by the quantum junction may not be sufficient to drag the heavy junction out of its minimum. Hence, we have to investigate the shape of the potential $v(\varphi_1,\varphi_2)$ after the phase slip in φ_2, i.e., nearby the point ($\varphi_1\gtrsim\arcsin j$, $\varphi_2\approx 2\pi$), and check whether the barrier against a classical decay (mainly along φ_1) has disappeared; this is identical to the calculation of the critical current of a SQUID with a trapped flux.[25,26]

We first determine the position of the minimum by solving the equations

$$\partial_{\varphi_1}v(\varphi_1,\varphi_2)=\sin(\varphi_1)-j+k(\varphi_1-\varphi_2)=0, \tag{7}$$

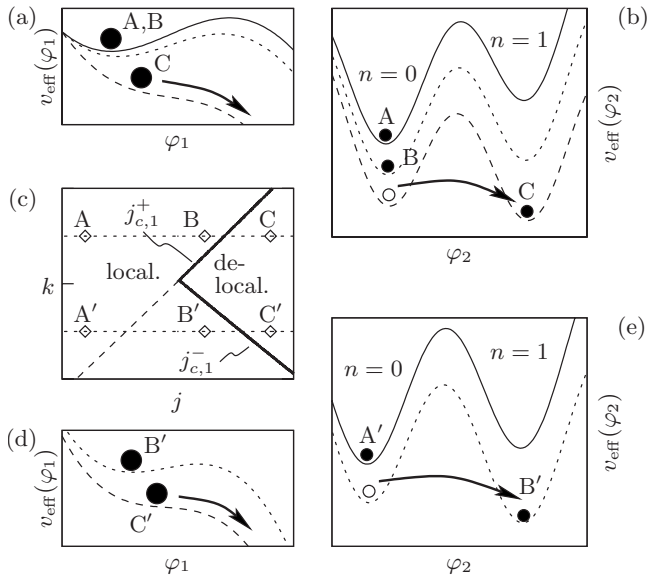

FIG. 4. Illustration of the assembly of $j_c(k)$ from the segments $j^+_{c,1}(k)$, Eq. (6), and $j^-_{c,1}(k)$, Eq. (11). In (c), the relevant region of the j-k plane is shown. At A, the quantum junction [see (b)] has relaxed to the initial minimum ($n=0$) and the classical junction is localized in a stable minimum [see (a)]. Increasing the bias current j and approaching B, the potential barrier confining the classical phase in $v_{\rm eff}(\varphi_1)$ is only slightly reduced. As $j>j^+_{c,1}(k)$ (point C), the increase in j has deformed the effective potential $v_{\rm eff}(\varphi_2)$ as to allow a phase slip of φ_2 [see (b)]. The additional force it exerts on the classical junction immediately removes the barrier [see (a)] and delocalizes φ_1 at $j_c(k)=j^+_{c,1}(k)$. On the other hand, an increase in bias $j>j^+_{c,1}(k)$ from A′ to B′ at lower k leads to a phase slip of φ_2 [(see (e)], without delocalizing φ_1 [see (d)]. A further increase in j triggers a classical decay [see (d)] when crossing the critical line at $j_c(k)=j^-_{c,1}(k)$ (point C′).

$$\partial_{\varphi_2} v(\varphi_1,\varphi_2) = \sin(\varphi_2) - j - k(\varphi_1-\varphi_2) = 0, \tag{8}$$

for $\varphi_1 \gtrsim \arcsin j$ and $\varphi_2 \approx 2\pi$. At the critical coupling $k^-_{c,1}(j)$ the minimum should merge with a saddle and define an inflection point along some direction in the (φ_1,φ_2) plane. The resulting system of equations requires numerical solution and the result is shown in the inset of Fig. 5. However, within the interesting region at small coupling k we can find an approximate analytical solution: for $k \ll 1$, the side minimum of $v(\varphi_1,\varphi_2)$ becomes unstable predominantly along the φ_1 direction. Thus, the minimum disappears if

$$\partial^2_{\varphi_1} v(\varphi_1,\varphi_2) = \cos\varphi_1 + k = 0. \tag{9}$$

We choose the solution $\varphi_1 \approx \pi/2$ [we set $k=0$ and assume $0 \le \varphi_1 < 2\pi$, the other solution $\varphi_1 \approx 3\pi/2$ cannot solve Eq. (7) and is discarded]. Inserting φ_1 into the sum of Eqs. (7) and (8) yields the relation

$$\sin\varphi_2 \approx 2j - 1, \tag{10}$$

from which we find $\varphi_2 \approx 2\pi + \arcsin[2j-1]$ (the other solution $\varphi_2 \approx 3\pi - \arcsin[2j-1]$ is excluded since it describes a maximum along the φ_2 direction). Inserting φ_1 and φ_2 into Eq. (7), we find the condition

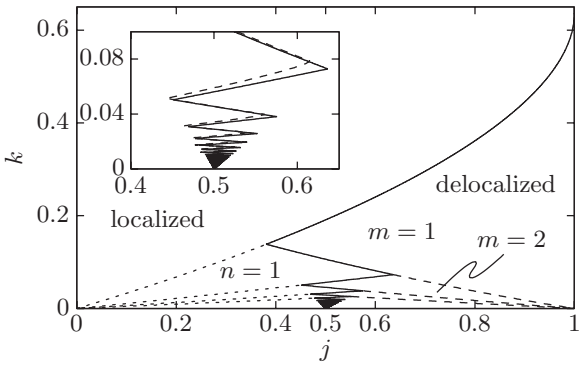

FIG. 5. Phase diagram of the dynamically asymmetric dc SQUID as a function of bias current $j=J/2J_c$ and inductive coupling $k=\Phi_0 c/2\pi L J_c$. Here, we assume strong damping $\alpha_{p,1} \gg 1$ and $\alpha_{p,2} > 1$. The effective critical current $j_c(k)$ (solid line) marks the boundary between a localized classical junction (lower bias $j<j_c$) and a delocalized classical junction ($j>j_c$), corresponding to a finite-voltage state of the SQUID. Branches with negative slope are determined by a classical instability (mainly along φ_1), while those with positive slope are determined by a quantum instability of the light junction. For $j<j_c(k)$, the dotted lines $j^+_{c,n}(k)$ mark the entry of flux through the quantum junction (the integer n approximately quantifies the flux through the ring in the stable state); these lines can be measured via monitoring of the flux threading the loop. For $j>j_c(k)$, dashed lines $j^-_{c,m}(k)$ mark the minimum number m of flux units necessary to delocalize the classical junction. Inset shows a comparison between the approximate result, Eqs. (13) and (14) (solid line), and the exact numerical result (dashed).

$$k^-_{c,1}(j) \approx \frac{1-j}{(3/2)\pi + \arcsin(2j-1)}. \tag{11}$$

For $k>k^-_{c,1}(j)$ no barrier blocks the motion of φ_1 after the phase slip in φ_2 and a classical decay of φ_1 is enabled, thus completing the Münchhausen decay. This scenario is described by the sequence A, B, C in Fig. 4(c). For $k<k^-_{c,1}(j)$ the force after the phase slips is too small and an additional increase in j is necessary to drive the system overcritical, as illustrated by the sequence A′, B′, C′ in Figs. 4(c)–4(e). The increase in critical current with decreasing coupling defines a negative slope for $k^-_{c,1}(j)$.

We define the effective critical current $j_c(k)$ as the phase boundary between the stable region $[j<j_c(k)]$, where the Münchhausen decay is prohibited, and the delocalized phase $[j>j_c(k)]$. This critical line is assembled from the segments $j^\pm_{c,1}(k)$, the inverse functions of $k^\pm_{c,1}(j)$, Eqs. (6) and (11), respectively. Ramping up the current j at large values of k, we eventually cross $j^+_{c,1}(k)$. The phase slip of φ_2 immediately enables the classical decay of φ_1 and the system enters a running state, hence, $j_c(k)=j^+_{c,1}(k)$. At lower k, increasing j beyond $j^+_{c,1}(k)$ triggers a phase slip of φ_2, but the resulting force is too weak to delocalize φ_1. A further increase in j is necessary until, at $j=j^-_{c,1}(k)$, the minimum disappears and the Münchhausen decay proceeds, hence, $j_c(k)=j^-_{c,1}(k)$.

Following the above discussion, the system is stable for $j<j^-_{c,1}(k)$. Upon further decreasing k, however, more and more side minima in $v_{\rm eff}(\varphi_2)$ become accessible to the quantum junction. From Fig. 3 we notice that the different local

minima of $v_{\rm eff}(\varphi_2)$ are located near $\varphi_2 \approx 2\pi n$. They describe the state where a flux $\simeq n\Phi_0$ has entered the loop and we label them by the index n. Equation (6) is then straightforwardly generalized to the critical line $k^+_{c,n}(j)$ describing the entry of the nth fluxon. The nth phase slip of φ_2 occurs when the global minimum in $v_{\rm eff}(\varphi_2)$ shifts from $\varphi_2 \approx 2\pi(n-1)$ to $\varphi_2 \approx 2\pi n$. We can proceed analogously to the derivation of Eq. (6): let $\varphi_1^{\min,n-1}$ be the solution of Eqs. (7) and (8) near $\varphi_1 \gtrsim \arcsin j$, $\varphi_2 \approx 2\pi(n-1)$. In order to find the crossing in the height of the two minima we account for the relaxation of φ_1 and align the minimum of the shifted parabola $(\varphi_2 = \varphi_1^{\min,n-1} + j/k)$ with the midpoint between the two minima of the $-\cos\varphi_2$ potential $[\varphi_2 = (2n-1)\pi]$, hence $\varphi_1^{\min,n-1} + j/k = (2n-1)\pi$ and

$$k^+_{c,n}(j) = \frac{j}{(2n-1)\pi - \varphi_1^{\min,n-1}}. \tag{12}$$

A convenient approximation is made by ignoring the relaxation of φ_1, resulting in the expression

$$k^+_{c,n}(j) \approx \frac{j}{(2n-1)\pi - \arcsin j}. \tag{13}$$

Similarly, we can generalize Eq. (11) to a critical coupling $k^-_{c,n}(j)$, determining whether the resulting force at given fluxon index n is sufficient to delocalize φ_1. We then solve Eqs. (7) and (8) near $\varphi_1 \approx \arcsin j, \varphi_2 \approx 2\pi n$, proceed as in the derivation of Eq. (11), and find (for small $k \ll 1$)

$$k^-_{c,n}(j) \approx \frac{1-j}{(2n-1/2)\pi + \arcsin(2j-1)}. \tag{14}$$

The critical current line $j_c(k)$ is constructed from interchanging segments of $j^+_{c,n}(k)$ and $j^-_{c,n}(k)$, resulting in the dynamical phase diagram (Fig. 5). Note that the different natures of the decay, classical or quantum, associated with the two types of critical lines may allow for an experimental distinction: ramping the current past a +-type segment of $j_c(k)$ triggers a *quantum* decay with a broad histogram describing multiple measurements. A −-type segment of $j_c(k)$ triggers a *classical* decay with a sharp histogram (the quantum decay of φ_2 needs to have occurred already, which limits the ramping speed before reaching the critical line). Note that the lines $j^+_{c,n}(k)$ are detectable throughout all the stable portion of the phase diagram, e.g., via a measurement of the flux threading the loop (the flux increases by approximately 1 flux unit upon crossing the dotted lines in Fig. 5).

The phase diagram in Fig. 5 shows that the critical line $j_c(k)$ approaches the value $\frac{1}{2}$ for $k \to 0$. This is understood from analyzing Eqs. (13) and (14) for large n and small k, providing the relations $k^+_{c,n}(j) \approx j/2n\pi$ and $k^-_{c,n}(j) \approx (1-j)/2n\pi$, respectively. Equating the two conditions gives $j_c \approx 0.5$. From a physical point of view, this result can be easily explained: the decay of φ_2 proceeds toward the bottom of the parabola in $v_{\rm eff}(\varphi_2)$; for $k \to 0$, the current through the quantum junction then approaches zero, $J_2 \propto \sin\varphi_2 \approx 0$. Consequently, all current is redirected through the classical junction 1, with the effective bias now increased to $J_1 = 2jJ_c$.

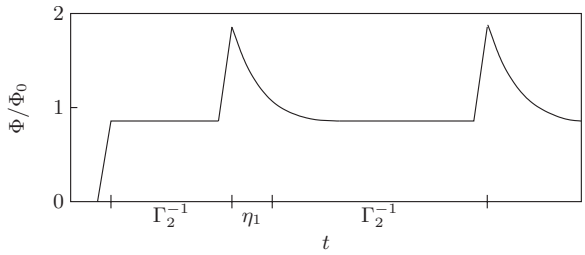

FIG. 6. Sketch of a time trace of the flux threading the SQUID loop during the decay process of φ_1 and φ_2 at $j > j_c(k)$ [cf. Fig. 2(b)]. The flux increases by approximately 1 flux unit each time the quantum junction decays; this process then involves the tunneling rate Γ_2 of φ_2, Eq. (15). The additional flux leaves the loop again within the time interval $\sim \eta_1$ as the classical junction relaxes dissipatively to the next minimum.

Junction 1 thus turns dissipative at $j = \frac{1}{2}$, the critical current of a single junction but half the critical current of the dc SQUID.

The dynamical phase diagram, Fig. 5, can be tested experimentally through a measurement of the dc voltage drop across the device. The second Josephson relation[1] tells that the time-averaged voltage through junction i, $\langle V_i \rangle_t \propto \langle \dot{\varphi}_i \rangle_t$. Inspecting Fig. 2(b), we understand that the continuous iteration of quantum and classical decays of the light phase variable and the heavy phase variable generate the nonzero averages $\langle \dot{\varphi}_1 \rangle_t = \langle \dot{\varphi}_2 \rangle_t$ for $j > j_c(k)$. The time averages over the two phases are equal since, during one full iteration of the decay cycle, *both* phases advance by 2π. Thus, the voltage drop over the total device $\langle V \rangle_t = \langle V_1 \rangle_t = \langle V_2 \rangle_t$. For the overdamped setup described above, the voltage drop is small, as strong damping reduces the tunneling rate determining the average "velocities" $\langle \dot{\varphi}_i \rangle_t$. This is particularly true close to the critical line, where the variable φ_2 needs to tunnel in the "flat" part of $v_{\rm eff}(\varphi_2)$. The decay process is faster for weak damping and thus generates a larger voltage signal—we discuss this situation in Sec. IV.

Another characteristic signal of the Münchhausen decay is the time trace of the magnetic flux threading the SQUID loop during the alternating decay of the two phases (see Figs. 2(b) and 6 for an illustration). Such time traces exhibit two characteristic time scales: one is due to the tunneling of the quantum junction involving the rate Γ_2 separating subsequent peaks of flux entry into the loop and the other is due to the classical relaxation of the heavy junction and involves the dissipative time $\sim \eta_1$ describing the flux exit and return to the low-flux state of the loop. At small k and small effective bias between two minima,

$$\frac{\Gamma_2^{(n)}}{\omega_{0,2}} \approx \frac{\hbar\omega_{0,2}E_{c,2}}{E_J^2}\left(\frac{R_Q}{\pi R_2}\right)^{7/2}(j - j^+_{c,n})^{2R_Q/R_2 - 1}, \tag{15}$$

with $R_Q = h/4e^2$.[27]

IV. WEAK DAMPING

The behavior of the system for weak damping $\alpha_{LC,2} \ll 1$, $\alpha_{p,i} \ll 1$ is quite similar to the one encountered before, while

the (small) differences strongly depend on the many system parameters and their associated time scales. Let us neglect dissipative effects for the moment. Bearing in mind the limit of large C_1/C_2, we can exploit the adiabatic separation of fast and slow degrees of freedom, i.e., we first consider the fast problem for the quantum junction,

$$\mathcal{H}_2\Psi_l(\varphi_2) = \varepsilon_l\Psi_l(\varphi_2), \tag{16}$$

with the reduced Hamiltonian [cf. Eq. (1)]

$$\mathcal{H}_2 = -4E_{c,2}\partial_{\varphi_2}^2 + E_J v_{\text{eff}}[\varphi_1](\varphi_2) \tag{17}$$

defined at *fixed* φ_1. Equation (16) establishes the dynamics of the light variable φ_2 and we can find the energies $\varepsilon_l(\varphi_1)$. These act as effective potentials for the heavy degree of freedom φ_1, e.g., assuming the quantum junction to reside in a state $|l\rangle$, $\langle\varphi_2|l\rangle = \Psi_l(\varphi_2)$, the effective potential for φ_1 is given by $\varepsilon_l(\varphi_1)$. Typical examples for the effective potentials $\varepsilon_0(\varphi_1)$ (ground state) and $\varepsilon_1(\varphi_1)$ (first excited state) are shown in Fig. 7.

In the dissipative situation, we could derive the phase diagram from simply analyzing the potential $v(\varphi_1,\varphi_2)$; here, instead, we first determine which states l of the light junction are relevant and then analyze the dynamics of φ_1 in the resulting effective potential [e.g., Fig. 7(a)] defined via $\varepsilon_l(\varphi_1)$, thus determining whether the heavy junction stays localized or enters a running state. Both tasks strongly depend on the various time scales involved. We start with the time scale of the "external control," the rate at which the bias j is ramped. Whereas the case of strong damping excluded the presence of kinetic energy in the system, this is no longer the case here. The importance of the ramping rate then comes about through the amount of energy which is transferred to the two degrees of freedom. The change in j translates to a change in the potential $v(\varphi_1,\varphi_2)$ with a rate on the order of $\partial_t j$. The ramping can be adiabatic, in which case no energy is given to the system, or instantaneous, where the amount of transferred energy is maximal. Intermediate types of ramping will not be discussed.

The adiabatic separation of time scales requires a large capacitance ratio $C_1 \gg C_2$. For $\omega_{p,1} \ll \omega_{p,2}$ the intravalley motions of the two junctions are separated. The (tunneling) motion of the light junction across valleys produces a stronger condition. Consider the tunneling splitting Δ_2 in the spectrum of $\mathcal{H}_2$ at an avoided level crossing [cf. Fig. 7(a)],

$$\Delta_2 \sim \hbar\omega_{p,2}\exp(-\gamma\sqrt{E_J/4E_{c,2}}), \tag{18}$$

with γ depending on the actual shape of the potential,

$$\gamma = \int_a^b d\varphi_2\sqrt{v_{\text{eff}}(\varphi_2) - E_0/E_J} \tag{19}$$

in the quasiclassical approximation. Here, E_0 is the ground-state energy in the well and a and b are the left and right classical turning points, respectively, $v_{\text{eff}}(\varphi_2=a) = v_{\text{eff}}(b) = E_0/E_J$. The tunneling gap Δ_2 then is relevant when analyzing the motion of the classical junction (φ_1) in the effective potential given by $\varepsilon_l(\varphi_1)$. If the motion of φ_1 is sufficiently slow, its passage along an avoided crossing in the spectrum of $\mathcal{H}_2$ is adiabatic and φ_1 follows $\varepsilon_l(\varphi_1)$ through the anti-

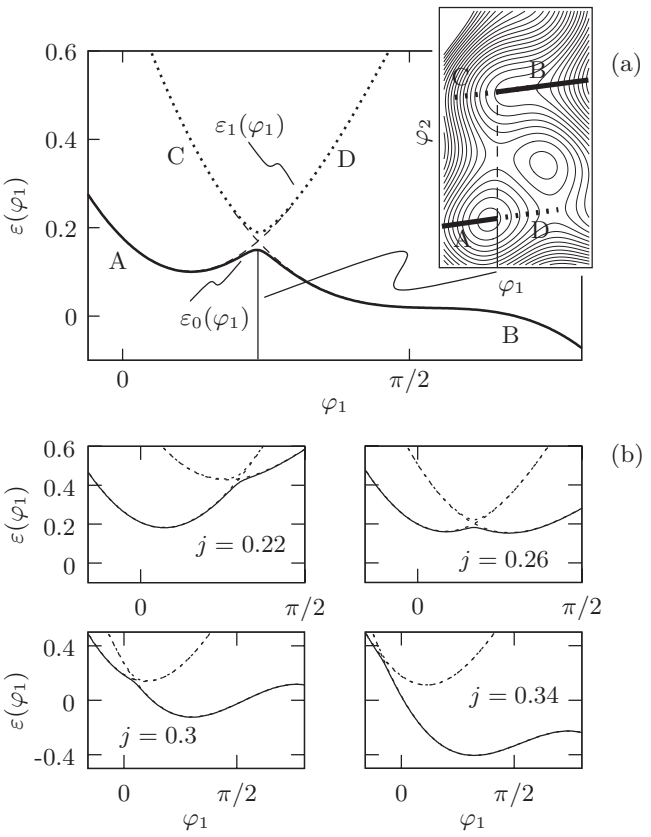

FIG. 7. Illustration of the effective potential for the heavy phase φ_1, generated by the two lowest levels of the light phase. In (a), the situation for $k=0.15$, $j=0.36$ is shown. The avoided level crossing $2\Delta_2$ in the spectrum of the light junction is reflected in the effective potentials $\varepsilon_0(\varphi_1)$ (solid) and $\varepsilon_1(\varphi_1)$ (dotted) for the heavy junction. Inset illustrates the two-dimensional path $[\varphi_1, \varphi_2^{\min,0/1}(\varphi_1)]$ in $v(\varphi_1,\varphi_2)$ corresponding to $\varepsilon_0(\varphi_1)$ (solid, A/B) and $\varepsilon_1(\varphi_1)$ (dotted, C/D); the upward/downward jump along φ_2 to the next minimum corresponds to the avoided crossing in $\varepsilon(\varphi_1)$. (b) Series of $\varepsilon_0(\varphi_1)$ (solid) and $\varepsilon_1(\varphi_1)$ (dotted) for various values of j at $k=0.1$. Increasing j shifts the position of the avoided crossing in $\varepsilon(\varphi_1)$ to the left. Its transition past $\varphi_1^{\min}$ (between $j=0.26$ and $j=0.3$) corresponds to crossing the line $j_{c,1}^{+}(k)$ and implies the decay of the quantum junction to the next local minimum. Note that in the present case the newly formed minimum is stable (a point of type B′ in Fig. 4).

crossing [cf. the trajectory A→B in Fig. 7(a)], i.e., the phase φ_2 tunnels to the next adjacent minimum. On the other hand, if the motion of φ_1 is fast, the state of the quantum junction undergoes Landau-Zener tunneling [cf. the trajectory A→D in Fig. 7(a); the light junction then remains trapped in its local well] and φ_1 follows the effective potential $\varepsilon_{l\pm1}(\varphi_1)$ after the avoided crossing. The probability p_{LZ} for Landau-Zener tunneling at an anticrossing of the two lowest levels of $\mathcal{H}_2$ is given by

$$p_{\text{LZ}} = \exp\left(-\frac{2\pi\Delta_2^2}{\hbar|d_t\varepsilon_{10}(t)|}\right), \tag{20}$$

where $\varepsilon_{10}(t) = \varepsilon_1(t) - \varepsilon_0(t)$ and d_t is the total time derivative. To estimate the rate of change in energy $d_t\varepsilon_{10}(t)$, we start from

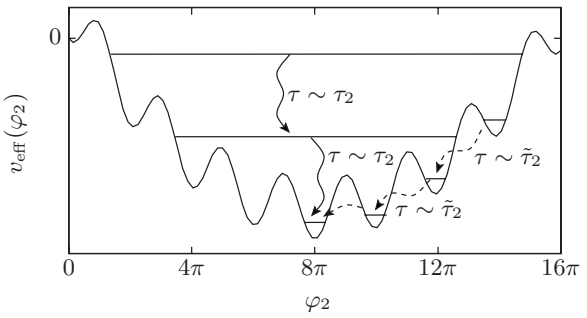

FIG. 8. Illustration of decay sequences of an excited superwell state of the quantum junction in the effective potential $v_{\rm eff}(\varphi_2)$, Eq. (3). Solid arrows indicate a decay sequence involving only states within the superwell with a typical decay time τ_2. Dashed arrows illustrate another (extreme) decay sequence, involving localized states in the side minima of $v_{\rm eff}(\varphi_2)$. The decay time then involves the typical lifetime $\tilde{\tau}_2 \gg \tau_2$ of local ground states within side wells.

$$\varepsilon_{10} \approx E_J[v(\varphi_1, \varphi_2^{\min,n+1}) - v(\varphi_1, \varphi_2^{\min,n})] \tag{21}$$

and find the time derivative

$$\begin{aligned} d_t\varepsilon_{10}(t) &= \partial_{\varphi_1}\varepsilon_{10}\dot{\varphi}_1 + E_J[\partial_{\varphi_2}v(\varphi_1,\varphi_2)|_{\varphi_2^{\min,n+1}}\partial_{\varphi_1}\varphi_2^{\min,n+1} \\ &\quad - \partial_{\varphi_2}v(\varphi_1,\varphi_2)|_{\varphi_2^{\min,n}}\partial_{\varphi_1}\varphi_2^{\min,n}]\dot{\varphi}_1 \\ &= kE_J(\varphi_2^{\min,n} - \varphi_2^{\min,n+1})\dot{\varphi}_1, \end{aligned} \tag{22}$$

where we have used that $\partial_{\varphi_2}v(\varphi_1,\varphi_2)$ vanishes at the minima $\varphi_2^{\min,n}$ and only the term originating from the coupling term in $v(\varphi_1,\varphi_2)$ is relevant. Since $\dot{\varphi}_1$ is at most of order $\omega_{0,1}$, we obtain the estimate $d_t\varepsilon_{10} \sim 2\pi k\omega_{0,1}E_J$. The smallness of $p_{\rm LZ}$, guaranteeing adiabatic motion of the classical junction (this requires a correspondingly large C_1), then follows from

$$k\frac{E_J}{\Delta_2}\frac{\hbar\omega_{0,1}}{\Delta_2} \sim k\sqrt{\frac{E_{c_1}}{E_{c_2}}}\sqrt{\frac{E_J}{E_{c_2}}}\exp\left(2\gamma\sqrt{\frac{E_J}{4E_{c_2}}}\right) \ll 1. \tag{23}$$

Let us now include the effect of (weak) dissipation as the relaxation of the quantum degree of freedom φ_2 is an important element in our discussion. The dissipation described by the normal resistance R in the RCSJ equation of motion [cf. Eq. (1)] leads to typical finite lifetimes $\tau_2 \sim RC_2 = 1/2\alpha_2\omega_{p,2}$ of the excited states $|l\rangle$ of the quantum junction.[28] A much longer lifetime $\tilde{\tau}_2$ shows up if the quantum junction is trapped in a local ground state of a side well in $v_{\rm eff}(\varphi_2)$ [cf. Fig. 8]. The decay then is protected through a large barrier E_b, enhancing the typical lifetime to a value $\tilde{\tau}_2$, with $\tau_2 \ll \tilde{\tau}_2 \propto \exp(2\gamma\sqrt{E_J/4E_{c,2}})$.[29] Thus, there are two (extreme) ways how a highly exited state in the superwell of $v_{\rm eff}(\varphi_2)$ can decay (see Fig. 8): either via states within the superwell involving the typical lifetime τ_2 or via states involving a tunneling process, resulting in an exponentially larger decay time on the order of $\tilde{\tau}_2$.

In the following, we investigate three regimes and derive the corresponding effective critical current $j_c(k)$. We begin with the case of adiabatic ramping (Sec. IV A), where we assume that the ramping is slower than the typical relaxation time of the heavy junction and the time scales between φ_1 and φ_2 separate, i.e., inequality (23) holds. We show that the critical current $j_c(k)$ obtained in the dissipative case (Sec. III) is only slightly altered due to the (small) finite amount of kinetic energy the classical junction can store. Next, we discuss the case of fast ramping (Sec. IV B), where the phase φ_1 remains effectively "frozen" during the current ramping and quite an appreciable amount of potential energy is converted to kinetic energy in the motion of the classical junction, leading to a pronounced reduction in $j_c(k)$. Both discussions require a very large value of $C_1/C_2 \to \infty$ to guarantee the absence of Landau-Zener tunneling due to the motion of φ_1. In the last part of this section (Sec. IV C), we discuss the consequences of an intermediate ratio C_1/C_2, where probabilistic effects show up in the dynamical phase diagram. Then, φ_2 can remain trapped in a localized state in a side well during the motion and liberation of the heavy junction. The probabilistic effects emerging for this situation change the nature of the phase diagram qualitatively.

A. Adiabatic ramping of the bias current

We start from the system with fixed coupling k at $j=0$ and consider a state localized at $\varphi_1=\varphi_2=0$. We assume slow current ramping on the dissipative time scale of the classical junction's motion

$$\partial_t j \ll 1/\tau_1, \tag{24}$$

where $\tau_1 \sim RC_1$ denotes the classical relaxation time of the heavy junction. The inequalities in Eq. (24) (slow ramping) and Eq. (23) (slow motion of φ_1) guarantee that the quantum junction remains in the global ground state, while the classical junction follows its local ground state near $\varphi_1 = \arcsin j$.

The effective potential for the heavy junction then is determined by the ground-state energy $\varepsilon_0(\varphi_1)$. In our estimate

$$\varepsilon_0(\varphi_1) \approx E_J v[\varphi_1, \varphi_2^{\rm glob}(\varphi_1)], \tag{25}$$

we neglect the correction due to the ground-state energy $E_0 \approx \hbar\omega_{p,2}/2$ (as measured from the bottom of the potential) of the light junction;[30] the phase $\varphi_2^{\rm glob}(\varphi_1)$ refers to the global minimum of the light junction. Furthermore, we ignore the small splitting $2\Delta_2$ at the avoided level crossing [cf. Fig. 7(a)], replacing it with a sharp kink.

With the above approximations, the force acting on the heavy junction originates from the classical force exerted by the quantum junction residing in the global minimum. The situation is thus the same as in the strong damping regime: the "flux-entry lines" $j_{c,n}^{+}(k)$, marking the current, where the light junction is allowed to tunnel, are still given by Eq. (12). When the classical junction has relaxed to the bottom of a minimum, that minimum has to disappear in order for φ_1 to enter the running state. Given the expression (25) for $\varepsilon_0(\varphi_1)$, the local minimum in $\varepsilon_0(\varphi_1)$ corresponding to the nth side minimum in $v_{\rm eff}(\varphi_1,\varphi_2)$ turns into an inflection point at $j = j_{c,n}^{-}(k)$, Eq. (14). This condition again agrees with the one for strong damping.

A difference to the previous dissipative situation is given by the possibility to transform potential into kinetic energy. Ramping j at fixed k past the flux-entry line $j_{c,n}^{+}(k)$ triggers a

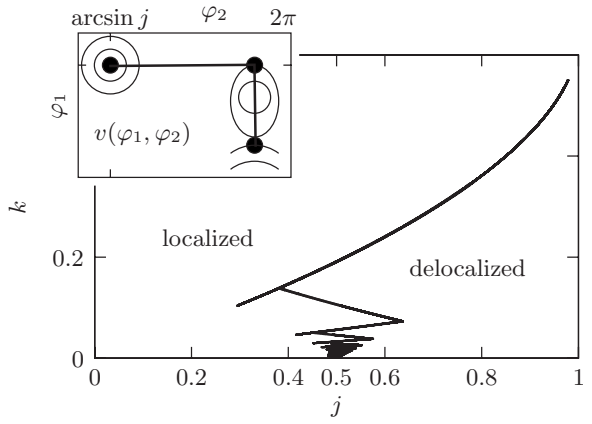

FIG. 9. Phase diagram of the dynamically asymmetric dc SQUID for weak damping and adiabatic ramping, $(\partial_t j \ll \tau_1^{-1})$. The critical line $j_c(k)$ is nearly identical with the one in the strong damping case, but is hysteretic along extensions of the critical lines $j_{c,n}^{+}(k)$. These are due to the nonzero kinetic energy acquired by the classical junction when sliding down in the new well formed after the tunneling of φ_2 at $j_{c,n}^{+}(k)$ and allowing φ_1 to surmount a residual potential barrier in the effective potential $\varepsilon_0(\varphi_1)$. Inset illustrates the condition determining the termination point of the hysteretic line along $j_{c,1}^{+}(k)$. The three solid dots mark points of equal potential energies; the energy gained by the classical junction due to the phase slip of φ_2 just suffices to climb the top of the remaining barrier along φ_1.

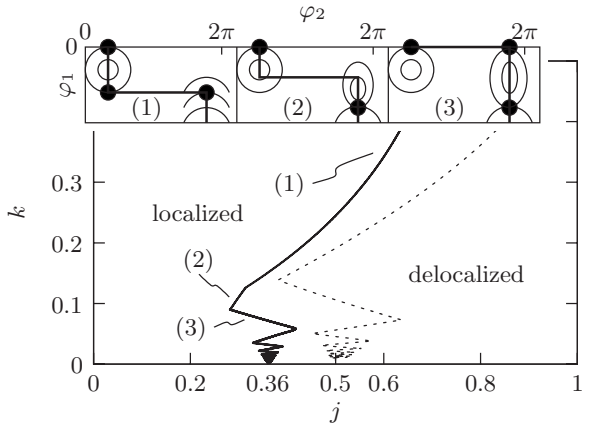

FIG. 10. Effective critical current $j_c(k)$ (solid) of the current-biased dc SQUID with strongly asymmetric parameters as a function of bias current j and inverse inductance $k \propto 1/L$. We assume instantaneous ramping of the bias j and a strictly classical and adiabatically slow (as compared to the dynamics of the quantum junction) motion of the weakly damped heavy degree of freedom φ_1. For comparison, the critical line of the dissipative case is also displayed (dashed line). Inset illustrates the three segments constituting the first part of $j_c(k)$, where solid dots indicate points of equal potential energy. Inset (3) shows the situation right at the tip between segments (2) and (3).

phase slip in φ_2 and deforms the potential well in $\varepsilon_0(\varphi_1)$ for the classical junction. The latter finds itself on the slope of the well and gains kinetic energy while sliding down toward the new minimum. The classical junction then may enter a running state if this kinetic energy gain is sufficient to surpass the barrier blocking the newly formed (nth) minimum. Different from the overdamped case, the system then exhibits hysteretic behavior, as illustrated in the dynamical phase diagram Fig. 9, where the running state can be entered along extensions of the $j_{c,n}^{+}(k)$ line away from the phase boundary. The point where these extensions terminate is determined by the condition that the energy right after the tunneling of φ_2 is equal to the energy at the top of the barrier, as illustrated in the inset of Fig. 9. If the coupling k is too small to lower the barrier sufficiently [cf. Fig. 7(b)], the state of the heavy junction upon reaching $j=j_{c,n}^{+}(k)$ is transformed into a localized excited state of the newly formed potential well in $\varepsilon_0(\varphi_1)$. Given the slow ramping $\partial_t j \ll \tau_1^{-1}$, the heavy junction relaxes to the ground state of the well and a further increase in j is necessary to remove the barrier completely, hence the critical line jumps forward to $j_c(k)=j_{c,n}^{-}(k)$.

B. Fast ramping of the bias current

We now turn to the case $\partial_t j \gg \omega_{p,1}$, where the ramping of j is instantaneous with respect to the (massive) dynamics of the heavy junction; the final current j has to remain below ~ 0.7 since fast ramping beyond this value allows the classical junction to overcome the potential barriers through conversion of potential to kinetic energy. Furthermore, we study the setting, where $\omega_{p,1} \ll \tau_2^{-1}, \tilde{\tau}_2^{-1}$; the quantum junction then has relaxed to the ground state (at $\varphi_2^{\min,n}$) in the effective potential $v_{\text{eff}}(\varphi_2)$ before any motion of the heavy junction sets in. Hence, initially, the effective potential for the classical junction is given by the ground-state energy $\varepsilon_0(\varphi_1)$. The absence of Landau-Zener tunneling [due to the inequality in Eq. (23)] then assures that the effective potential is given by $\varepsilon_0(\varphi_1)$ during the entire motion of the classical junction.

We then can find the criterion for φ_1 to enter a running state: during the fast ramping of the current j, the heavy junction remains frozen at $\varphi_1=0$. We have to check whether the potential energy of the heavy junction is sufficient to overcome all barriers in $\varepsilon_0(\varphi_1>0)$, i.e., we have to inspect if the maximum of $\varepsilon_0(\varphi_1)$ in the interval $0<\varphi_1<2\pi$ is realized at $\varphi_1=0$. As soon as this condition applies, the classical junction becomes delocalized. This analysis has to be performed numerically and the result is displayed in Fig. 10. As a first overall result, we note that the critical current is shifted to lower values due to the instantaneous change in the effective potential for φ_1 by the fast ramping of the current and by the quantum decay of φ_2, allowing the heavy junction to transform potential into kinetic energy.

Another prominent change is in the form of the transition line, specifically, the "cut" of the first tip of $j_c(k)$. The first segment at large values of k (cf. Fig. 10) corresponds to the conventional case for a +-type line; the criterion for delocalization involves the full conversion of potential to kinetic energy of the heavy junction and the subsequent tunneling of the quantum junction right at the turning point of the classical junction [cf. inset (1) of Fig. 10]. Following the $j_c^{+}(k)$ line further with decreasing j, we reach a point where the potential energy of the classical junction after the phase slip event is no longer sufficient to overcome the next barrier and an additional increase in j is required to provide the missing

energy. Segment (2) then involves partial conversion of the initial potential energy within the two wells before and after the phase slip event. Finally, moving along the segment (2) toward lower k the value of φ_1 where the phase slip occurs decreases and finally reaches $\varphi_1=0$ [cf. Fig. 10, inset (3)]. The critical line then continues along the third segment which is of the typical −-type, with the quantum junction undergoing tunneling before the classical junction starts moving. After tunneling, a large current is required to lower the barrier in the cosine potential of the classical junction [cf. Fig. 10, inset (3)]. Note that the differentiation between positively sloped segments of type (1) and type (2) persists to segments determined by a higher fluxon index n, although the difference is invisible on the scale of Fig. 10.

C. Intermediate ratios of C_1/C_2: Probabilistic effects

Above, we have assumed the limit of very large ratios C_1/C_2 and explained the generic behavior of the system. In the case where this ratio assumes an intermediate value, one may enter a new, interesting, and qualitatively different dynamical regime, where the classical junction is pulled out of its metastable state more effectively. This efficient liberation is realized when the quantum junction attains a high-energy state residing at the opposite side of the parabolic potential (large values of φ_2 in Fig. 8) and holds on to it while dragging the heavy junction out of its metastable state. This requires a fast[31] current ramping $\partial_t j \gg 1/\tilde{\tau}_2$ (on the scale of the intervalley motion of the light junction), pushing the quantum junction to high potential energies during the ramp-up process. Furthermore, the condition $\omega_{p,1} \gg 1/\tilde{\tau}_2$ has to be satisfied to allow for motion of the heavy junction before relaxation of the quantum junction (from a side-well local ground state) back to the global minimum; this condition defines the largeness of the capacitance ratio C_1/C_2 required for this regime.

In order to simplify the situation, we assume a (weak) finite damping of the classical junction, $\omega_{p,1}^{-1} \ll \tau_1 < \tilde{\tau}_2$, assuring that the classical junction relaxes before tunneling of the quantum junction (this assumption is merely a convenience, allowing us to ignore the availability of kinetic energy for the classical junction upon fast ramping). We then start from the local ground state of the original potential well at $\varphi_1=\varphi_2=\arcsin j$. The decay proceeds in the direction of φ_2 in the effective potential $v_{\mathrm{eff}}[\arcsin j](\varphi_2)$ and can end up in any of the lower local ground states for the quantum junction. We denote the energy of the local ground state of the quantum junction in the nth well by $\tilde{\varepsilon}_0^n$ (not to be confused with ε_n, the nth excited state in the spectrum of the quantum junction). We estimate these energies as

$$\tilde{\varepsilon}_0^n(\varphi_1) \approx v(\varphi_1, \varphi_2^{\min,n}), \tag{26}$$

where $\varphi_2^{\min,n}(\varphi_1)$ is the solution to Eq. (8) near $\varphi_2 \approx 2\pi n$ at fixed φ_1 and we have neglected the zero-point energy $\hbar\omega_{p,2}/2$.

The dynamics of φ_1 depends strongly on the fluxon index n of the state of the quantum junction after the decay: the larger n, the stronger is the force on φ_1 facilitating its escape. We can define two extreme values for the critical current: a lower limit $j_c^{(1)}(k)$ arising from the largest attainable fluxon index n and an upper limit $j_c^{(2)}(k)$ associated with the index n of the global minimum of the quantum junction. We estimate the maximal index n by comparing the energy of the state of the quantum junction before its initial decay to the height of the barrier blocking the access to the nth minimum. The numerical solution of the relation

$$v_{\mathrm{eff}}[\varphi_1 = \arcsin j](\varphi_2 = \arcsin j) = v_{\mathrm{eff}}(\varphi_2^{\max,n}), \tag{27}$$

with $\varphi_2^{\max,n}$ the solution to Eq. (8) near $\varphi_2^{\max} \approx (2n-1)\pi$ at $\varphi_1=\arcsin j$ provides us with the line $j_{c,n}^{(1)+}(k)$. The subsequent stability analysis of φ_1 generates the lines $j_{c,n}^{(1)-}(k)$; their combination into $j_c^{(1)}(k)$ is displayed in Fig. 11.

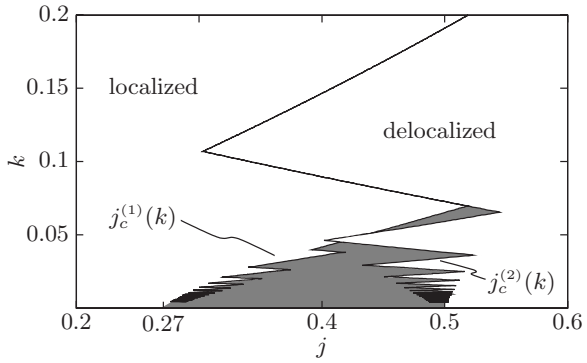

FIG. 11. Effective critical currents of the dynamically asymmetric SQUID for $\tilde{\tau}_2 \gg \omega_{p1}^{-1}$ and fast ramping. The system always turns resistive for $j > j_c^{(2)}(k)$ but never turns resistive for $j < j_c^{(1)}(k)$. For $j_c^{(1)} < j < j_c^{(2)}$ the delocalization of the system is determined by the statistical nature of the decay process of the quantum junction involving the side minima.

The shape of $j_c^{(2)}(k)$ is found as described before: we determine the index n of the global minimum of $v_{\mathrm{eff}}(\varphi_2)$ and deduce the motion of φ_1 in the effective potential $\tilde{\varepsilon}_0^n(\varphi_1)$. The reduction in critical current due to the massive dynamics of φ_1 is not as pronounced as in Fig. 10, since the maximal critical current $j_c^{(2)}(k)$ involves the process, where the classical junction dissipates most of its kinetic energy. The quantum junction decays to the $(n-1)$ fluxon state, the classical junction relaxes to its local minimum near $\varphi_1 \gtrless \arcsin j$, whereupon the quantum junction decays further to its global ground state with fluxon index n. Only the potential energy gained by the classical junction in the last step can be transformed to kinetic energy, making the resulting line shown in Fig. 11 differ from $j_c(k)$ in the overdamped case (Fig. 5).

The two critical lines $j_c^{(1)}(k)$ and $j_c^{(2)}(k)$ define a broad intermediate regime (see the gray area in Fig. 11) where the decay of the system is of probabilistic nature: whereas no Münchhausen decay is possible for $j < j_c^{(1)}(k)$, the decay of the system in the intermediate regime depends on which minimum the quantum junction φ_2 decays to. For $j > j_c^{(2)}(k)$ the system is always bound to decay.

The critical line $j_c^{(2)}(k)$ crosses twice the critical line $j_c^{(1)}(k)$ near $k \approx 0.5$ and for $n=2$. This special situation arises when the most distant accessible minimum and the global minimum are neighbors (with indices $n=2$ and $n=1$) and hence strongly interrelated. With decreasing k, both the

height of the maximum near $\varphi_2 \approx 3\pi$ [determining $j_c^{(1)}(k)$] and the position of the minimum at $\varphi_2 \approx 4\pi$ ($n=2$) with respect to the one at $\varphi_2 \approx 2\pi$ [$n=1$; the competition between these minima defines $j_c^{(2)}(k)$] are lowered. The latter effect is slightly stronger, leading to the crossing of the lines under a small angle. Upon further lowering of k, the relevant fluxon index for $j_c^{(1)}(k)$ increases twice as fast as for $j_c^{(2)}(k)$, preventing any further crossings of the critical lines.

To guarantee reasonable time scales in the experiment requires a fast quantum dynamics near the global minimum, hence the ratio $E_J/\hbar\omega_{p,2}$ should be small, of order unity. For a fast ramping, this is in conflict with the requirement of large $\tilde{\tau}_2$ in all side wells; as a result, not all reachable side minima may be relevant for the dynamics of φ_1 (i.e., $\tilde{\tau}_2 \gg \omega_{p,1}^{-1}$ does not hold), effectively shifting the lower critical current $j_c^{(1)}(k)$ to larger values.

So far we have neglected any quantum corrections for the variable φ_1; however, with a finite ratio C_1/C_2 such corrections may become relevant. Modifications due to quantum fluctuations in the heavy degree of freedom are twofold: on the one hand, we have disregarded the tunneling of φ_1 through a small residual barrier, leading to a broadening of all lines of the $-$-type. On the other hand, we have assumed the dynamics of φ_2 to occur in the effective potential $v_{\text{eff}}[\varphi_1](\varphi_2)$, with φ_1 fixed, while for a finite value of C_1 the ground-state wave function of the heavy junction acquires a finite width on the order of $\delta\varphi_1 \sim (8E_{c1}/E_J)^{1/4}$. This leads to a broadening of all lines of the +-type, which can be interpreted as φ_1 taking part in the tunneling of φ_2.

V. EXPERIMENTAL IMPLEMENTATION

The running state following a Münchhausen decay is associated with a finite time-averaged voltage across the device. The above results can therefore be tested experimentally, e.g., by measuring the voltage drop as a function of the applied bias current J and of the inductance L of the SQUID.

In an experiment in the weak-damping regime (Sec. IV), the dynamical asymmetry of the SQUID could be implemented by shunting one of the two junctions with an external capacitance.[32] Capacitive shunts on the order of a few pF can be fabricated nowadays[33] while typical small junctions have capacitances on the order of a fF.[11,14] Thus, ratios $C_1/C_2 \sim 10^3$ are feasible already today.

Apart from a general reduction in the critical current below the classical value of $2J_c$, the major manifestation of the Münchhausen effect is the shape of the effective critical current $j_c(k)$ in the $J-L^{-1}$ plane at low values of $k<0.2$. The latter is determined by the total inductance of the loop $L=L_{\text{geo}}+L_{\text{kin}}$, comprising the geometric (L_{geo}) and kinetic (L_{kin}) inductances of the loop. The former is on the order of the loop perimeter and accounts for the magnetic field energy. The kinetic inductance relates to the geometric quantity via $L_{\text{kin}} \sim L_{\text{geo}}\lambda^2/r^2$, with r the radius of the wire and λ denoting the superconducting penetration depth. Usually, the inductance is dominated by its geometric part. However, a large inductance, as desired for our setup, can be installed by using a thin wire.

Detecting the shape of the critical line $j_c(k)$ in the $J-L^{-1}$ plane requires changing the coupling $k \propto L^{-1}$. Unfortunately, the inductance is fixed after fabrication; its modification may require the installation of a diamagnetic shield or a change in sample geometry. An efficient way of tracing the (local) shape of the critical current line in an experiment is obtained by applying an external magnetic flux Φ_e to the sample, in which case the potential Eq. (2) has to be replaced by

$$v(\varphi_1,\varphi_2) = 1-\cos\varphi_1 + 1-\cos\varphi_2 - j(\varphi_1+\varphi_2) + \frac{k}{2}(\varphi_1-\varphi_2-2\pi\Phi_e/\Phi_0)^2. \tag{28}$$

The critical current j_c then can be studied as a function of Φ_e and uncovers the changeover between two branches $j_{c,n}^{+}(k)$ and $j_{c,n}^{-}(k)$. Due to the periodicity in Φ_e, only one pair of branches at fixed n can be observed; other portions of the critical line with different n could then be traced out by changing the sample geometry or adding a shield. Note the universal shape of the rescaled curve $j_c(k)$ for devices with junctions of equal coupling E_J; this feature can be exploited provided that junctions of equal coupling can be fabricated and their critical current can be measured.

The analysis including an external flux Φ_e proceeds in the same way as before: a change in k altering the opening angle of the parabola in $v(\varphi_1,\varphi_2)$ is replaced by a shift in the parabola's position due to the applied flux Φ_e. As an illustration, we discuss here the most simple case of an overdamped dynamics, analogous to Sec. III. In a first step, the system relaxes to the ground state at the minimum of the potential $v(\varphi_1,\varphi_2)$, Eq. (28), as given by the solutions $\varphi_1^{\min}$, $\varphi_2^{\min}$ of

$$\sin(\varphi_1^{\min}) - j + k\left(\varphi_1^{\min}-\varphi_2^{\min}-2\pi\frac{\Phi_e}{\Phi_0}\right) = 0, \tag{29}$$

$$\sin(\varphi_2^{\min}) - j - k\left(\varphi_1^{\min}-\varphi_2^{\min}-2\pi\frac{\Phi_e}{\Phi_0}\right) = 0 \tag{30}$$

near $\varphi_1^{\min} \approx \varphi_2^{\min} \approx 0$. The critical line $j_{c,n}^{+}(\Phi_e)$ then derives from the condition

$$k \approx \frac{j}{(2n-1)\pi - \varphi_1^{\min}(\Phi_e) + 2\pi\Phi_e/\Phi_0}, \tag{31}$$

where both the shift of the parabola $v_{\text{eff}}(\varphi_2)$ by $2\pi\Phi_e/\Phi_0$ and the flux dependence of $\varphi_1^{\min}$ are accounted for. Similarly, Eq. (14) for $k_{c,n}^{-}(j)$ is changed to

$$k \approx \frac{1-j}{(2n-1/2)\pi + \arcsin(2j-1) + 2\pi\Phi_e/\Phi_0}, \tag{32}$$

from which we find the critical lines $j_{c,n}^{-}(\Phi_e)$. The results of Eqs. (29)–(32) are invariant under the shifts $\Phi_e/\Phi_0 \to \Phi_e/\Phi_0 \pm 1$ and $n \to (n \mp 1)$. The Münchhausen decay thus can be studied within a finite interval, e.g., $\Phi_e/\Phi_0 \in [-0.5, 0.5]$, and the resulting phase diagram is displayed in Fig. 12.

Biasing the SQUID with an external magnetic flux has a convenient side effect: for negative flux Φ_e, the crossing point of $j_{c,n}^{+}(k)$ and $j_{c,n}^{-}(k)$ is shifted to larger values of k and

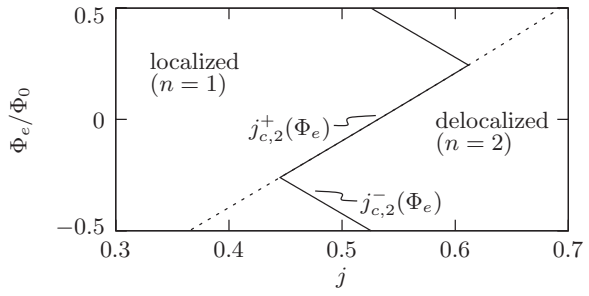

FIG. 12. Phase diagram of the dynamically asymmetric SQUID in the strong damping case as a function of the externally applied flux Φ_e and bias current j. Here, the coupling $k \propto L^{-1}$ is fixed at a value $k=0.06$; the critical lines in the diagram correspond to $n=2$. The critical line is periodic in Φ_e with a period Φ_0, a consequence of the invariance under the replacements $\Phi_e/\Phi_0 \to \Phi_e/\Phi_0 \pm 1$ and $n \to (n \mp 1)$.

the tunneling barrier for φ_2 is lowered, allowing to study the Münchhausen effect using a SQUID with considerably smaller inductance and hence smaller size.

Additional experiments can be performed which test the classical and quantum natures of the critical current branches or the extension of $j^+_{c,n}(k)$ away from the critical line (see Fig. 5). As previously discussed in Sec. III, the different nature of the decay on branches of $j_c(k)$ with different slope is accessible to experimental verification. Since the decay is ultimately of quantum nature on positively sloped branches $[j^+_{c,n}(k)]$, broad time-bin histograms of multiple measurements are expected. On negatively sloped branches $[j^-_{c,n}(k)]$, where the decay is ultimately classical and deterministic, the resulting histograms are more narrow. In carrying out such an experiment with an underdamped sample, care has to be taken in letting the system relax in the last stable state before crossing $j_c(k)$.

In another type of experiment, the time trace of the flux threading the loop in the finite-voltage state can be measured (see the illustration Fig. 6). Furthermore, the flux charging of the loop upon crossing a $j^+_{c,n}(k)$ line not constituting part of the critical line (dotted line in Fig. 5) can easily be measured, without stringent requirements regarding the time resolution of the experiment. Likewise, the discharging upon crossing a $j^-_{c,n}(k)$ part of $j_c(k)$ manifests itself as a reduction in the time-averaged flux.

VI. CONCLUSION

We have shown how a system consisting of a quantum degree of freedom coupled to a classical one, implemented with a two-junction SQUID, can perform a complex decay process out of a zero-voltage state involving quantum tunneling of the light junction and classical motion of the heavy junction. We have analyzed the cases of strong and weak damping for different methods of preparation (fast and slow ramping) and for various ratios of the capacitances C_1/C_2 and have found the effective critical current $j_c(k)$ exhibiting a common characteristic shape. Its zig-zag-like structure originates in two competing effects: while the number n of flux units which can enter the SQUID is increased with decreasing k, the current redirected over the heavy junction at given n is decreased. For junctions with equal critical currents, the critical line approaches the value $j_c(k \to 0) \to \frac{1}{2}$ in the dissipative case; asymmetries in the critical currents of the two junctions lead to a shift of the critical line $j_c(k)$ to values straddling the critical current of the heavy junction. Going over from dissipative to massive dynamics, the kinetic energy stored in the system allows to better overcome the potential barriers and the critical line shifts to smaller values of j; furthermore, hysteretic effects, similar to the situation encountered for underdamped junctions, and even probabilistic behavior may show up.

ACKNOWLEDGMENTS

We thank A. Larkin, A. Ustinov, G. Lesovik, A. Lebedev, A. Wallraff, and E. Zeldov for interesting discussions and acknowledge support of the Fonds National Suisse through MaNEP.

[1] B. D. Josephson, Phys. Lett. **1**, 251 (1962).
[2] We use modified Gaussian units, where C and L are measured in units of length.
[3] R. F. Voss and R. A. Webb, Phys. Rev. Lett. **47**, 265 (1981).
[4] A. O. Caldeira and A. J. Leggett, Phys. Rev. Lett. **46**, 211 (1981).
[5] A. O. Caldeira and A. J. Leggett, Ann. Phys. (N.Y.) **149**, 374 (1983).
[6] M. H. Devoret, J. M. Martinis, and J. Clarke, Phys. Rev. Lett. **55**, 1908 (1985).
[7] J. M. Martinis, M. H. Devoret, and J. Clarke, Phys. Rev. Lett. **55**, 1543 (1985).
[8] J. M. Martinis, M. H. Devoret, and J. Clarke, Phys. Rev. B **35**, 4682 (1987).
[9] S. Chakravarty and A. J. Leggett, Phys. Rev. Lett. **52**, 5 (1984).
[10] A. J. Leggett, S. Chakravarty, A. T. Dorsey, M. P. A. Fisher, A. Garg, and W. Zwerger, Rev. Mod. Phys. **59**, 1 (1987).
[11] Y. Nakamura, C. D. Chen, and J. S. Tsai, Phys. Rev. Lett. **79**, 2328 (1997).
[12] Y. Nakamura, Y. A. Pashkin, and J. S. Tsai, Nature (London) **398**, 786 (1999).
[13] J. R. Friedman, V. Patel, W. Chen, S. K. Tolpygo, and J. E. Lukens, Nature (London) **406**, 43 (2000).
[14] C. H. van der Wal, A. C. J. ter Haar, F. K. Wilhelm, R. N. Schouten, C. J. P. M. Harmans, T. P. Orlando, S. Lloyd, and J. E. Mooij, Science **290**, 773 (2000).
[15] I. Chiorescu, Y. Nakamura, C. J. P. M. Harmans, and J. E. Mooij, Science **299**, 1869 (2003).
[16] S.-X. Li, Y. Yu, Y. Zhang, W. Qiu, S. Han, and Z. Wang, Phys. Rev. Lett. **89**, 098301 (2002).
[17] F. Balestro, J. Claudon, J. P. Pekola, and O. Buisson, Phys. Rev. Lett. **91**, 158301 (2003).

[18] Y.-C. Chen, J. Low Temp. Phys. **65**, 133 (1986).
[19] B. I. Ivlev and Y. N. Ovchinnikov, Sov. Phys. JETP **66**, 378 (1987).
[20] C. Morais Smith, B. Ivlev, and G. Blatter, Phys. Rev. B **49**, 4033 (1994).
[21] A similar setup with one tunable small (s) and one large (l) Josephson junction was used previously as a qubit (s) with integrated readout (l) (Refs. 34–36).
[22] Dissipation will only act in such a way as to further decrease the tunneling rate (Ref. 5).
[23] A. U. Thomann, V. B. Geshkenbein, and G. Blatter, Physica C **468**, 705 (2008).
[24] O. Hallatschek, Diploma thesis, ETH Zurich, 2000.
[25] W.-T. Tsang and T. V. Duzer, J. Appl. Phys. **46**, 4573 (1975).
[26] V. Lefevre-Seguin, E. Turlot, C. Urbina, D. Esteve, and M. H. Devoret, Phys. Rev. B **46**, 5507 (1992).
[27] S. E. Korshunov, Sov. Phys. JETP **65**, 1025 (1987).
[28] D. Esteve, M. H. Devoret, and J. M. Martinis, Phys. Rev. B **34**, 158 (1986).
[29] D. V. Averin, J. R. Friedman, and J. E. Lukens, Phys. Rev. B **62**, 11802 (2000).
[30] While the correction E_0 might not be immaterial, its dependence on φ_1 is small.
[31] When the ramping is slow, the modifications with respect to the discussion in Sec. IV A are negligible: due to the slow ramping, the quantum junction remains always in its ground state and hence the classical junction moves adiabatically in the effective potential $\varepsilon_0(\varphi_1)$ created by the quantum junction. The resulting critical current $j_c(k)$ is identical to the one presented in Fig. 9.
[32] M. Steffen, M. Ansmann, R. McDermott, N. Katz, R. C. Bialczak, E. Lucero, M. Neeley, E. M. Weig, A. N. Cleland, and J. M. Martinis, Phys. Rev. Lett. **97**, 050502 (2006).
[33] R. C. Bialczak, R. McDermott, M. Ansmann, M. Hofheinz, N. Katz, E. Lucero, M. Neeley, A. D. O'Connell, H. Wang, A. N. Cleland, and J. M. Martinis, Phys. Rev. Lett. **99**, 187006 (2007).
[34] F. Chiarello, P. Carelli, M. G. Castellano, C. Cosmelli, L. Gangemi, R. Leoni, S. Poletto, D. Simeone, and G. Torrioli, Supercond. Sci. Technol. **18**, 1370 (2005).
[35] M. G. Castellano, F. Chiarello, R. Leoni, G. Torrioli, P. Carelli, C. Cosmelli, M. Di Bucchianico, and D. Simeone, IEEE Trans. Appl. Supercond. **15**, 849 (2005).
[36] F. Chiarello, P. Carelli, M. G. Castellano, M. Cirillo, C. Cosmelli, G. Frossati, N. Gronbech-Jensen, F. Mattioli, S. Poletto, G. Torrioli, and A. de Waard, IEEE Trans. Appl. Supercond. **17**, 124 (2007).